Proceedings of ALGORITMY 2005
pp. 73–82

NUMERICAL MODELING OF SHALLOW FLOWS INCLUDING BOTTOM TOPOGRAPHY AND FRICTION EFFECTS

MÁRIA LUKÁČOVÁ-MEDVIĎOVÁ*

Abstract. The aim of the paper is numerical modeling of the shallow water equation with source terms by genuinely multdimensional finite volume evolution Galerkin schemes. The shallow water system, or its one-dimensional analogy the Saint-Venant equation, is used extensively for numerical simulation of natural rivers. Mathematically the shallow water system belongs to the class of balance laws. A special treatment of the source terms describing the bottom topography as well as frictions effects is necessary in order to reflect their balance with the gradients of fluxes. We present behaviour of our new well-balance FVEG scheme for several benchmark test problems and compare our results with those obtained by the finite element scheme of Teschke et al. used for practical river simulations [13].

Key words. shallow water equations, finite volume evolution Galerkin method, river simulations, well-balanced scheme, hyperbolic balance laws

AMS subject classifications. 65L05, 65M06, 35L45, 35L65, 65M25, 65M15

1. Introduction. Description of natural river processes is very complex. The main aim is to determine the water level at a specific place and time. Reliable mathematical models as well as robust, fast and accurate numerical simulations are very important for prediction of floods and have large economical impact. One of the main difficulty of the reliable calculation is the determination of the friction which counteracts the river flows [13]. Numerical simulation of natural river flows is based on the two-dimensional shallow water equations, in practice even its one-dimensional analogy is often used. The shallow water system consists of the continuity equation and the momentum equations

$$\boldsymbol{u}_t + \boldsymbol{f}_1(\boldsymbol{u})_x + \boldsymbol{f}_2(\boldsymbol{u})_y = \boldsymbol{b}(\boldsymbol{u}), \tag{1.1}$$

where

$$\boldsymbol{u} = \begin{pmatrix} h \\ hu \\ hv \end{pmatrix}, \ \boldsymbol{f}_1(\boldsymbol{u}) = \begin{pmatrix} hu \\ hu^2 + \frac{1}{2}gh^2 \\ huv \end{pmatrix},$$
$$\boldsymbol{f}_2(\boldsymbol{u}) = \begin{pmatrix} hv \\ huv \\ hv^2 + \frac{1}{2}gh^2 \end{pmatrix}, \ \boldsymbol{b}(\boldsymbol{u}) = \begin{pmatrix} 0 \\ -gh(b_x + S_f(u)) \\ -gh(b_y + S_f(v)) \end{pmatrix}.$$

Here h denotes the water depth, u, v are vertically averaged velocity components in $x-$ and $y-$ direction, g stands for the gravitational constant, $b = b(x, y)$ denotes the bottom topography and $S_f(u), S_f(v)$ are the friction terms in $x-$ and $y-$ directions. The determination of the friction slope S_f is a very complex problem. The bottom composition of a river varies very rapidly, especially when vegetation is taken into account. In the literature several methods in order to determine the friction slope can

*Arbeitsbereich Mathematik, University of Technology Hamburg, Schwarzenbergstrasse 95, 21073 Hamburg, Germany (lukacova@tu-harburg.de).

be found, cf., e.g. [13]. Basis for our calculation is the friction law of Darcy-Weisbach. Thus, the friction slope S_f is calculated by, see, e.g. [14],

$$S_f(u) = \frac{\lambda u \sqrt{u^2+v^2}}{8g\, r_{hy}}, \quad S_f(v) = \frac{\lambda v \sqrt{u^2+v^2}}{8g\, r_{hy}}, \tag{1.2}$$

where r_{hy} denotes the hydrodynamical radius and λ stays for the so-called resistance value, which is determined according to the simplified form of the Colebrook-White relation

$$\frac{1}{\sqrt{\lambda}} = -2.03\log\left(\frac{k_s/r_{hy}}{14.84}\right).$$

Here k_s denotes the friction parameter, which depends on the composition of the river bottom. Typically, k_s can vary from 1 mm for beton until 300 mm for bottom with dense vegetation.

2. Finite volume evolution Galerkin scheme. System of the shallow water equations (1.1) belongs to the class of nonlinear hyperbolic balance laws. In our recent works [7], [8], [9] we have proposed a new genuinely multidimensional finite volume evolution Galerkin method (FVEG), which is used to solve numerically nonlinear hyperbolic conservation laws. The method is based on the theory of bicharacteristics, which is combined with the finite volume framework. It can be also viewed as a predictor-corrector scheme; in the predictor step data are evolved along the bichracteristics, or along the bicharacteristic cone, in order to determine approximate solution on cell interfaces. In the corrector step the finite volume update is done. Thus, in our finite volume method we do not use any one-dimensional approximate Riemann solver, instead the intermediate solution on cell-interfaces is computed by means of an approximate evolution operator. The reader is referred to [2], [5], [11] and the references therein for other recent genuinely multidimensional methods. Numerical comparisons with other well-known schemes illustrate high global accuracy of the FVEG schemes. For example the second order FVEG scheme is six times more accurate that the Lax-Wendroff scheme as well as the LeVeque wave propagation algorithm [5], whereas the computational costs are comparable with the LeVeque scheme, which belongs also to the class of genuinely multidimensional methods.

One possible and simple way to solve a system of balance laws is to apply the operator splitting approach and solve separately the resulting homogenous system of hyperbolic conservation laws, e.g. by using the finite volume evolution Galerkin scheme, and the system of ordinary differetial equations, which includes the right-hand-side source terms. However, this can lead to the structural deficiencies and strong oscillations in the solutions, especially when stationary solutions or their small perturbations are to be computed numerically. In fact, most of the geophysical flows, including river flows, are nearly stationary flows. We say that a flow is stationary if

$$\frac{\mathrm{d}u}{\mathrm{d}t} \equiv \frac{\partial u}{\partial t} + u\frac{\partial u}{\partial x} + v\frac{\partial u}{\partial y} = 0, \quad \frac{\mathrm{d}v}{\mathrm{d}t} = 0.$$

In this case the gradient of fluxes is balanced with the right-hand side source term, i.e. we have the following balance condition in the x-direction $\partial_x(gh^2/2) = -gh(b_x + S_f(u))$. Assume that $R(u)$ is a primitive to $S_f(u)$. Then the balance condition can be rewritten as $gh(h+b+R(u))_x = 0$. An analogous condition holds in the $y-$direction. These *equilibrium conditons* yield the well-balanced approximation of the

source term. The resulting schemes are called *the well-balanced schemes*, cf., e.g. [1], [3], [4], [6] and the references therein for other well-balanced schemes in literaure.

Our aim is to generalize the finite volume evolution Galerkin scheme to the balance laws and derive the well-balance FVEG scheme. We follow our recent work presented in [10] and include moreover a suitable approximation of the friction terms, which are particularly important for reliable river flow simulations.

Our computational domain Ω wil be divided into a finite number of regular finite volumes $\Omega_{ij} = [x_{i-\frac{1}{2}}, x_{i+\frac{1}{2}}] \times [y_{j-\frac{1}{2}}, y_{j+\frac{1}{2}}] = [x_i - \hbar/2, x_i + \hbar/2] \times [y_j - \hbar/2, y_j + \hbar/2]$, $i, j \in \mathbb{Z}$, $\hbar$ is a mesh step. Further, we denote by $\boldsymbol{U}_{ij}^n$ the piecewise constant approximate solution on a mesh cell Ω_{ij} at time t_n and start with initial approximations obtained by the integral averages $\boldsymbol{U}_{ij}^0 = \int_{\Omega_{ij}} \boldsymbol{U}(\cdot, 0)$. The finite volume evolution Galerkin scheme can be formulated as follows

$$\boldsymbol{U}^{n+1} = \boldsymbol{U}^n - \frac{\Delta t}{\hbar} \sum_{k=1}^{2} \delta_{x_k} \bar{\boldsymbol{f}}_k^{n+1/2} + \boldsymbol{B}^{n+1/2}, \tag{2.1}$$

where Δt is a time step, δ_{x_k} stays for the central difference operator in the x_k-direction, $k = 1, 2$, and $\bar{\boldsymbol{f}}_k^{n+1/2}$ represents an approximation to the edge flux at the intermediate time level $t_n + \Delta t/2$. Further $\boldsymbol{B}^{n+1/2}$ stands for the approximation of the source term $\boldsymbol{b}$. The cell interface fluxes $\bar{\boldsymbol{f}}_k^{n+1/2}$ are evolved using an approximate evolution operator denoted by $E_{\Delta t/2}$ to $t_n + \Delta t/2$ and averaged along the cell interface edge denoted by $\mathcal{E}$, i.e.

$$\bar{\boldsymbol{f}}_k^{n+1/2} := \frac{1}{\hbar} \int_{\mathcal{E}} \boldsymbol{f}_k (E_{\Delta t/2} \boldsymbol{U}^n) \mathrm{d}S. \tag{2.2}$$

The well-balanced approximate evolution operator $E_{\Delta t/2}$ for system (1.1) will be given in the Section 3.

2.1. A well-balanced approximation of the source terms. As already mentioned above we want to approximate source terms in the finite volume update in such a way that the balance bewteen the source terms and the gradient of fluxes will be exactly preserved. This can be done by approximating the source term by using its values on interfaces, cf. [12].

Let us consider a stationary flow, i.e.

$$\begin{aligned} &\frac{\mathrm{d}u}{\mathrm{d}t} = 0, \quad \frac{\mathrm{d}v}{\mathrm{d}t} = 0, \\ &gh(h + b + R(u))_x = 0, \quad gh(h + b + R(v))_y = 0. \end{aligned} \tag{2.3}$$

Note that a stationary steady state, the so-called lake at rest, i.e. $u = 0 = v$, and $h + b =$ const., is a special equilibrium state, that is included here.

Assume that (2.3) holds. In order to derive a well-balanced approximation of the source term we should first realize, that the flux difference in the FV update formula, cf. second equation of (2.1), can be equivalently rewritten in the following way

$$\begin{aligned} &\frac{g}{2\hbar^2} \int_{y_{i-1/2}}^{y_{i+1/2}} \left((h_{i+1/2}^{n+1/2})^2 - (h_{i-1/2}^{n+1/2})^2 \right) \mathrm{d}S_y \\ &\qquad = \frac{g}{2\hbar^2} \int_{y_{i-1/2}}^{y_{i+1/2}} \left(h_{i+1/2}^{n+1/2} + h_{i-1/2}^{n+1/2} \right) \left(h_{i+1/2}^{n+1/2} - h_{i-1/2}^{n+1/2} \right) \mathrm{d}S_y. \end{aligned} \tag{2.4}$$

In order to preserve the equilibrium condition $gh(h+b+R(u))_x = 0$ we need to approximate h by an average of cell interface values and $(h+b+R(u))_x$ by a central difference. Therefore, we define the well-balanced approximation of the source term in the following way

$$\frac{1}{\hbar^2}\int_{\Omega_{ij}} B_2(\boldsymbol{U}^{n+1/2}) = \frac{1}{\hbar^2}\int_{x_{i-1/2}}^{x_{i+1/2}}\int_{y_{i-1/2}}^{y_{i+1/2}} -gh^{n+1/2}(b_x^{n+1/2}+R_x^{n+1/2})$$
$$\approx \frac{-g}{\hbar}\int_{y_{i-1/2}}^{y_{i+1/2}} \frac{h_{i+1/2}^{n+1/2}+h_{i-1/2}^{n+1/2}}{2}\,\frac{(b_{i+1/2}+R_{i+1/2}^{n+1/2})-(b_{i-1/2}+R_{i-1/2}^{n+1/2})}{\hbar}\mathrm{d}S_y.$$

Integrals along vertical cell interfaces are approximated by the Simpson rule similarly to the cell interface integration used in (2.4). An analogous approximation of the source term is used also in the third equation for the $y-$ direction.

3. Well-balanced approximate evolution operator. In order to derive the exact integral equations, which describe time evolution of the solution, it is suitble to work with the system (1.1) written in primitive variables $\boldsymbol{w} = (h,u,v)^T$, i.e.

$$\boldsymbol{w}_t + \boldsymbol{A}_1(\boldsymbol{w})\boldsymbol{w}_x + \boldsymbol{A}_2(\boldsymbol{w})\boldsymbol{w}_y = \boldsymbol{t}(\boldsymbol{w}), \tag{3.1}$$

$$\boldsymbol{A}_1 = \begin{pmatrix} u & h & 0 \\ g & u & 0 \\ 0 & 0 & u \end{pmatrix}, \quad \boldsymbol{A}_2 = \begin{pmatrix} v & 0 & h \\ 0 & v & 0 \\ g & 0 & v \end{pmatrix}, \quad \boldsymbol{t} = \begin{pmatrix} 0 \\ -g(b_x+S_f(u)) \\ -g(b_y+S_f(v)) \end{pmatrix}.$$

This is a simple form appropriate for working with characteristics away from shocks. Note that the approximate evolution operator based on (3.1) is only used in the predictor step. In the corrector step the finite volume update using the conservative variables is done. Therefore shocks will be resolved correctly.

Now we explore the hyperbolic structure of the homogenous part of (3.1) and use theory of bicharacteritics. In an analogous way as in [8], for the Euler equations, and in [7], for the homogeneous shallow water equations, we obtain the following exact integral equations

$$\begin{aligned} h(P) = {} & \frac{1}{2\pi}\int_0^{2\pi} h(Q) - \frac{\tilde{c}}{g}u(Q)\cos\theta - \frac{\tilde{c}}{g}v(Q)\sin\theta \mathrm{d}\theta \\ & -\frac{1}{2\pi}\int_{t_n}^{t_{n+1}} \frac{1}{t_{n+1}-\tilde{t}}\int_0^{2\pi}\frac{\tilde{c}}{g}\left(u(\tilde{Q})\cos\theta + v(\tilde{Q})\sin\theta\right)\mathrm{d}\theta\mathrm{d}\tilde{t} \\ & +\frac{1}{2\pi}\tilde{c}\int_{t_n}^{t_{n+1}}\int_0^{2\pi}\left(b_x(\tilde{Q})\cos\theta + b_y(\tilde{Q})\sin\theta\right)\mathrm{d}\theta\mathrm{d}\tilde{t} \\ & +\frac{1}{2\pi}\tilde{c}\int_{t_n}^{t_{n+1}}\int_0^{2\pi}\left(S_f(u(\tilde{Q}))\cos\theta + S_f(v(\tilde{Q}))\sin\theta\right)\mathrm{d}\theta\mathrm{d}\tilde{t} \end{aligned} \tag{3.2}$$

$$\begin{aligned} u(P) = {} & \frac{1}{2\pi}\int_0^{2\pi} -\frac{g}{\tilde{c}}h(Q)\cos\theta + u(Q)\cos^2\theta + v(Q)\sin\theta\cos\theta\,\mathrm{d}\theta \\ & +\frac{1}{2}u(Q_0) - \frac{1}{2}g\int_{t_n}^{t_{n+1}}\left(h_x(\tilde{Q}_0) + b_x(\tilde{Q}_0) + S_f(u(\tilde{Q}_0))\right)\mathrm{d}\tilde{t} \end{aligned} \tag{3.3}$$

$$
\begin{aligned}
&-\frac{1}{2\pi}g\int_{t_n}^{t_{n+1}}\int_0^{2\pi}\Big(b_x(\tilde{Q})\cos^2\theta+b_y(\tilde{Q})\cos\theta\sin\theta\Big)\,\mathrm{d}\theta\mathrm{d}\tilde{t}\\
&-\frac{1}{2\pi}g\int_{t_n}^{t_{n+1}}\int_0^{2\pi}\Big(S_f(u(\tilde{Q}))\cos^2\theta+S_f(v(\tilde{Q}))\cos\theta\sin\theta\Big)\,\mathrm{d}\theta\mathrm{d}\tilde{t}\\
&+\frac{1}{2\pi}\int_{t_n}^{t_{n+1}}\frac{1}{t_{n+1}-\tilde{t}}\int_0^{2\pi}\Big(u(\tilde{Q})\cos 2\theta+v(\tilde{Q})\sin 2\theta\Big)\,\mathrm{d}\theta\mathrm{d}\tilde{t}
\end{aligned}
$$

$$
\begin{aligned}
v\,(P)=\frac{1}{2\pi}\int_0^{2\pi}&-\frac{g}{\tilde{c}}h\,(Q)\sin\theta+u\,(Q)\sin\theta\cos\theta+v\,(Q)\sin^2\theta\,\mathrm{d}\theta\\
&+\frac{1}{2}v\,(Q_0)-\frac{1}{2}g\int_{t_n}^{t_{n+1}}\Big(h_y(\tilde{Q}_0)+b_y(\tilde{Q}_0)+S_f(v(\tilde{Q}_0))\Big)\,\mathrm{d}\tilde{t}\\
&-\frac{1}{2\pi}g\int_{t_n}^{t_{n+1}}\int_0^{2\pi}\Big(b_x(\tilde{Q})\sin\theta\cos\theta+b_y(\tilde{Q})\sin^2\theta\Big)\,\mathrm{d}\theta\mathrm{d}\tilde{t}\\
&-\frac{1}{2\pi}g\int_{t_n}^{t_{n+1}}\int_0^{2\pi}\Big(S_f(u(\tilde{Q}))\sin\theta\cos\theta+S_f(v(\tilde{Q}))\sin^2\theta\Big)\,\mathrm{d}\theta\mathrm{d}\tilde{t}\\
&+\frac{1}{2\pi}\int_{t_n}^{t_{n+1}}\frac{1}{t_{n+1}-\tilde{t}}\int_0^{2\pi}\Big(u(\tilde{Q})\sin 2\theta+v(\tilde{Q})\cos 2\theta\Big)\,\mathrm{d}\theta\mathrm{d}\tilde{t}.
\end{aligned}
\tag{3.4}
$$

Here $P=(x,y,t_{n+1})$ is the pick of the bicharacteristic cone, cf. Fig. 3.1, $Q_0=(x-\tilde{u}\Delta t, y-\tilde{v}\Delta t, t_n)$ denotes the center of the sonic circle, $\tilde{Q}_0=(x-\tilde{u}(t_n+\Delta t-\tilde{t}), y-\tilde{v}(t_n+\Delta t-\tilde{t}), \tilde{t})$, $\tilde{Q}=(x-\tilde{u}(t_n+\Delta t-\tilde{t})+c(t_n+\Delta t-\tilde{t})\cos\theta, y-\tilde{v}(t_n+\Delta t-\tilde{t})+c(t_n+\Delta t-\tilde{t})\sin\theta, \tilde{t})$ stays for arbitrary point on the mantle and $Q=Q(\tilde{t})\Big|_{\tilde{t}=t_n}$ denotes a point at the perimeter of the sonic circle at time t_n. The local velocities, which are obtained by averaging over the neighbouring values, are denoted by $\tilde{u},\tilde{v},\tilde{c}=\sqrt{g\tilde{h}}$.

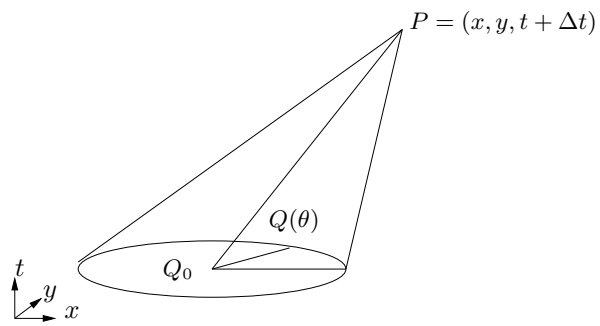

FIG. 3.1. *Bicharacteristic cone created by bicharacteristics through P and $Q=Q(\theta)$.*

3.1. Well-balanced approximation of exact integral equations. In order to use the exact integral equations in the numerical scheme we need to derive such an approximation, which preserves the equilibrium states exactly. In this paper we consider only the steady stationary states, i.e. $u=0=v, h+b=\text{const}$. More complex equilibrium states satysfying general equilibrium conditions (2.3) is a subject of our future study.

LEMMA 3.1. *The well-balanced approximation of the integral equations (3.2)-(3.4) reads*

$$
\begin{aligned}
(3.5)\quad h(P) = -b(P) &+ \frac{1}{2\pi}\int_0^{2\pi} \left(h(Q)+b(Q)\right) - \frac{\tilde{c}}{g}u(Q)\cos\theta - \frac{\tilde{c}}{g}v(Q)\sin\theta\, d\theta \\
&-\frac{1}{2\pi}\int_{t_n}^{t_{n+1}} \frac{1}{t_{n+1}-\tilde{t}}\int_0^{2\pi}\frac{\tilde{c}}{g}\left(u(\tilde{Q})\cos\theta + v(\tilde{Q})\sin\theta\right) d\theta\, d\tilde{t} \\
&+\frac{\tilde{c}\Delta t}{2\pi}\int_0^{2\pi}\left(S_f(u(Q))\cos\theta + S_f(v(Q))\sin\theta\right) d\theta + O\left(\Delta t^2\right),
\end{aligned}
$$

$$
\begin{aligned}
u(P) = \frac{1}{2\pi}\int_0^{2\pi} &-\frac{g}{\tilde{c}}\left(h(Q)+b(Q)\right)\cos\theta + u(Q)\cos^2\theta + v(Q)\sin\theta\cos\theta\, d\theta \\
(3.6)\qquad &+\frac{1}{2}u(Q_0) - \frac{1}{2\pi}\frac{g}{\tilde{c}}\int_{t_n}^{t_{n+1}}\frac{1}{t_{n+1}-\tilde{t}}\int_0^{2\pi}\left(h(\tilde{Q})+b(\tilde{Q})\right)\cos\theta\, d\theta\, d\tilde{t} \\
&+\frac{1}{2\pi}\int_{t_n}^{t_{n+1}}\frac{1}{t_{n+1}-\tilde{t}}\int_0^{2\pi}\left(u(\tilde{Q})\cos 2\theta + v(\tilde{Q})\sin 2\theta\right) d\theta\, d\tilde{t} \\
&-g\Delta t S_f(u(Q_0)) + O\left(\Delta t^2\right).
\end{aligned}
$$

The equation for the velocity v is analogous to that for u.

Proof.

First we deal with the *consistency* of the approximate equations (3.5)-(3.6). We only consider here the friction terms, the bottom elevation terms follows analogously as in [10]. The approximation of the friction terms in (3.2) is obtained using the rectangle rule in time, see (3.5). In (3.3) we apply for the friction terms integrated along the mantle the rectangle rule in time and the Taylor expansion on the sonic circle. This yields

$$
-\frac{g}{2\pi}\int_0^{2\pi}\int_{t_n}^{t_{n+1}}\left(S_f(u(\tilde{Q}))\cos\theta + S_f(v(\tilde{Q}))\sin\theta\right)\cos\theta\ \mathrm{d}\tilde{t}\mathrm{d}\theta =
$$

$$
= \frac{-g\Delta t}{2}S_f(u(Q_0)) + O(\Delta t^2).
$$

For the integral of the friction term along the middle bicharacteristic the rectangle rule in time is applied, which leads to

$$
-\frac{g}{2}\int_{t_n}^{t_{n+1}} S_f(u(\tilde{Q}_0))\,\mathrm{d}\tilde{t} = -\frac{g\Delta t}{2}S_f(u(Q_0)) + O(\Delta t^2).
$$

After substituting these approximations into (3.3) we obtain (3.6).

Now, let us show a *well-balanced* property of the approximate equations (3.5)-(3.6), i.e. we want to show that the steady stationary state $u = 0 = v$, $h + b = \text{const.}$ is preserved. Actually, it is easy to see from (3.5), and (1.2) that if $u(\cdot,t) = 0 = v(\cdot,t)$ and $h(\cdot,t)+b(\cdot) = \text{const.}$ for any $t \in [t_n, t_{n+1}]$, then $h(P)+b(P) \equiv h^{n+1}+b^{n+1} = \text{const.}$ Further, it follows from (3.6) that under the above assumptions, $u(\cdot,t) = 0 = v(\cdot,t)$ and $h(\cdot,t) + b(\cdot) = \text{const.}$ for any $t \in [t_n, t_{n+1}]$, we have $u(P) = u^{n+1} = 0$, and analogously $v(P) = v^{n+1} = 0$. Thus, the lake at rest is preserved, which concludes the proof. ∎

The next step is to approximate time integrals from t_n to t_{n+1} in order to obtain an explicit approximate evolution in time. This is done by means of the numerical quadratures which were proposed in [9]. These new quadrature rules are derived in such a way that any planar one-dimensional wave is calculated exactly. They are now used for approximation of all time integrals along mantle of the bicharacteristic cone.

Applying quadrature rules from [9] we obtain the following **well-balanced approximate evolution operator** E_Δ^{const} for piecewise constant functions

$$
\begin{aligned}
h\left(P\right) &= \frac{1}{2\pi}\int\limits_0^{2\pi}\left(h\left(Q\right)+b(Q)\right)-\frac{\tilde{c}}{g}u\left(Q\right)\operatorname{sgn}(\cos\theta)-\frac{\tilde{c}}{g}v\left(Q\right)\operatorname{sgn}(\sin\theta)\mathrm{d}\theta \\
&\quad -b(P)+\frac{\tilde{c}\Delta t}{2\pi}\int_0^{2\pi}\left(S_f(u(Q))\cos\theta+S_f(v(Q))\sin\theta\right)\mathrm{d}\theta+O\left(\Delta t^2\right), \\
u\left(P\right) &= \frac{1}{2\pi}\int\limits_0^{2\pi}-\frac{g}{\tilde{c}}\left(h\left(Q\right)+b\left(Q\right)\right)\operatorname{sgn}(\cos\theta)+u\left(Q\right)\left(\cos^2\theta+\frac{1}{2}\right) \\
&\quad +v\left(Q\right)\sin\theta\cos\theta d\theta-g\Delta t S_f(u(Q_0))+O\left(\Delta t^2\right). \qquad (3.7)
\end{aligned}
$$

If the continuous piecewise bilinear functions are used the **well-balanced approximate evolution operator**, which is denoted by E_Δ^{bilin}, reads

$$
\begin{aligned}
h\left(P\right) &= -b(P)+\left(h(Q_0)-b(Q_0)\right)+\frac{1}{4}\int\limits_0^{2\pi}\left(\left(h(Q)-h(Q_0)\right)+\left(b(Q)-b(Q_0)\right)\right)\mathrm{d}\theta \\
&\quad -\frac{1}{\pi}\int\limits_0^{2\pi}\left(\frac{\tilde{c}}{g}u(Q)\cos\theta+\frac{\tilde{c}}{g}v(Q)\sin\theta\right)\mathrm{d}\theta \\
&\quad +\frac{\tilde{c}\Delta t}{2\pi}\int_0^{2\pi}\left(S_f(u(Q))\cos\theta+S_f(v(Q))\sin\theta\right)\mathrm{d}\theta+O\left(\Delta t^2\right), \\
u\left(P\right) &= u(Q_0)-\frac{1}{\pi}\int\limits_0^{2\pi}\frac{g}{\tilde{c}}\left(h(Q)+b(Q)\right)\cos\theta\mathrm{d}\theta \\
&\quad +\frac{1}{4}\int\limits_0^{2\pi}\left(3u(Q)\cos^2\theta+3v(Q)\sin\theta\cos\theta-u(Q)-\frac{1}{2}u(Q_0)\right)\mathrm{d}\theta \qquad (3.8) \\
&\quad -g\Delta t S_f(u(Q_0))+O\left(\Delta t^2\right).
\end{aligned}
$$

Equations for the velocity v are analogous to those for u. The approximate evolution operators (3.7) and (3.8) are used in (2.2) in order to evolve fluxes along cell interfaces. Thus, the first order method is obtained using the approximate evolution operator E_Δ^{const}

$$
\bar{\boldsymbol{f}}_k^{n+1/2}=\frac{1}{\hbar}\int_{\mathcal{E}}\boldsymbol{f}_k(E_{\Delta t/2}^{const}\boldsymbol{U}^n)\mathrm{d}S, \qquad k=1,2,
$$

whereas in the second order FVEG scheme a suitable combination of the approximate evolution operator E_Δ^{bilin} and E_Δ^{const} is used. We apply E_Δ^{bilin} to evolve slopes and

E_{Δ}^{const} to evolve the corresponding constant part in order to preserve conservativity

$$\bar{\boldsymbol{f}}_k^{n+1/2} = \frac{1}{\bar{h}} \int_{\mathcal{E}} \boldsymbol{f}_k \Big(E_{\Delta t/2}^{bilin} R_h \boldsymbol{U}^n + E_{\Delta t/2}^{const} (1 - \mu_x^2 \mu_y^2) \boldsymbol{U}^n \Big) \mathrm{d}S.$$

Here $R_h \boldsymbol{U}$ denotes a continuous bilinear recovery and $\mu_x^2 U_{ij} = 1/4(U_{i+1,j} + 2U_{ij} + U_{i-1,j})$; an analogous notation is used for the $y-$direction.

4. Numerical experiments. In this chapter we demonstrate throughout the numerical experiments behaviour of our new well-balanced FVEG scheme.

Example 1: a balance test
In this example we illustrate the well-balanced property of the first as well as second order FVEG scheme. As a simple balance test we consider the shallow water system (1.1) with the bottom topography consisting of a hump

$$b(x,y) = \begin{cases} 0.25(\cos(10\pi(x-0.5))+1) & \text{if } |x-0.5| < 0.1,\ y \in [0,1], \\ 0 & \text{otherwise.} \end{cases}$$

We consider the flow without friction and set the friction parameter $k_s = 0$. The initial data are chosen as follows

$$h(x,y,0) = 1 - b(x,y), \quad u(x,y,0) = 0, \quad v(x,y,0) = 0.$$

The computational domain is $[0,1] \times [0,1]$ and the extrapolation boundary conditions are used. This initial value problem has the trivial stationary steady state solution $h(x,y,t) = 1 - b(x,y),\ u(x,y,t) = 0,\ v(x,y,t) = 0$ for all t. In Table 4.1 the L^1-errors for different times computed with the first order FVEG method, cf. (3.7), and with the second order FVEG method, cf. (3.8), are given. Although we have used a rather coarse mesh consisting of 20×20 mesh cells, it can be seen clearly that the FVEG scheme balances up to machine accuracy.

TABLE 4.1
The L^1-error of the well-balance FVEG scheme using 20×20 mesh cells. (Data computed by Marcus Kraft, TU Hamburg-Harburg)

Method	$t = 0.2$	$t = 1$	$t = 10$
first order FVEG	1.110223×10^{-17}	7.216450×10^{-17}	1.332268×10^{-16}
second order FVEG	2.775558×10^{-17}	5.551115×10^{-17}	4.440892×10^{-17}

Example 2: propagating waves with a bottom topography
In this example a trully two-dimensional problem of a small perturbances of a steady stationary state is simulated. The bottom topography is given by the function

$$b(x,y) = 0.8 \exp\Big(-5\,(x-0.9)^2 - 50\,(y-1)^2\Big) \tag{4.1}$$

and the initial data are

$$h(x,y,0) = \begin{cases} 1 - b(x,y) + \varepsilon & \text{if } 0.05 < x < 0.15, \\ 1 - b(x,y) & \text{otherwise,} \end{cases}$$

$$u(x,y,0) = v(x,y,0) = 0. \tag{4.2}$$

The parameter of small perturbation ε is set to 0.01. We consider here again flow without friction, i.e. $k_s = 0$. The computational domain is $[0, 2] \times [0.5, 1.5]$ and the absorbing extrapolation boundary conditions are used. In Figure 4.1 we present the solution computed on a 600×300 grid by the second order FVEG scheme with the minmod limiter. The values of the water depth h varies between 1 and 1.01. It should be pointed out that no oscillations appear in the solution as the wave propagate over the bottom hump. This will not be the case if the source term on the right-hand-side of (1.1) is not approximated in a well-balanced way. Our results are in a good agreement with other results presented in literature, cf., e.g., [4], [6].

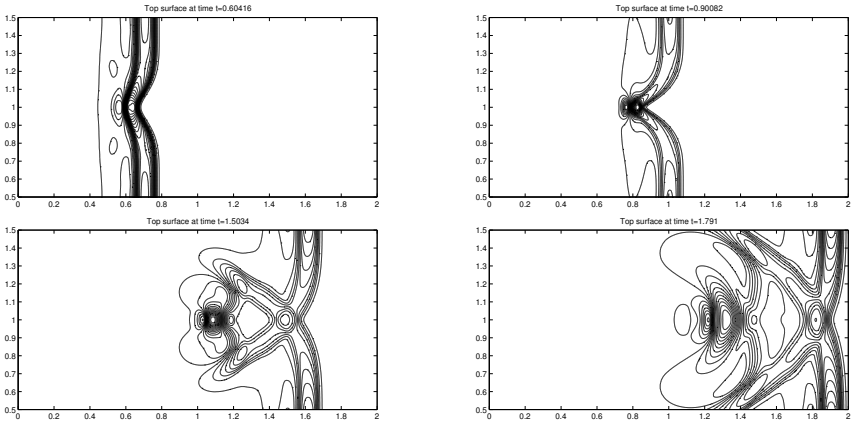

FIG. 4.1. *Propagation of small perturbances over an eliptic hump at various times;* $t = 0.6$ *(left above),* $t = 0.9$ *(right above),* $t = 1.5$ *(left below) and* $t = 1.8$ *(right below).*

Example 3: a channel flow with friction

In this example we simulate a flow in a regular rectangular channel of $\ell = 1\,km$ length and $w = 6\ m$ width. The bottom profile is given by

$$b(x, y) = \begin{cases} -0.001(x - 500) + 0.5 & \text{if } 0 < x < 500,\ y \in [0, 6], \\ 0.5 & \text{if } 500 < x < 1000,\ y \in [0, 6]. \end{cases}$$

The friction parameter of the bottom is set to $k_s = 0.1$. We take a steady state as the initial data, i.e. $h(x, y, 0) + b(x, y) = 2,\ u(x, y, 0) = 0 = v(x, y, 0)$.

At the inflow, i.e. $x = 0m$, the volume rate flow is taken to be $Q \equiv w\,h\,u = 3m^3s^{-1}$. The inflow velocity in the $y-$ direction is $0ms^{-1}$. At the outflow, i.e. $x = 1000m$, absorbing boundary conditions are imposed by extrapolating the data in the outer normal direction. In order to evaluate frictions slopes the hydraulic radius r_{hy} is to be computed. For a regular rectangular channel it is computed by the formula $r_{hy} = w\,h/(2h+b)$. The solution is evolved in time by the FVEG scheme until a steady state is obtained. The resulting numerical solution is compared with the results of Teschke computed by the finite element method applied to the one-dimensional steady shallow water equations (i.e. the Saint-Venant equation), cf. also [13], [14]. Our steady state is in a very good agreement with the results obtained by the finite element code, which is used for practical river flow simulations, see Figure 4.2. Moreover, our method is in general approximately four times faster than the above finite element scheme.

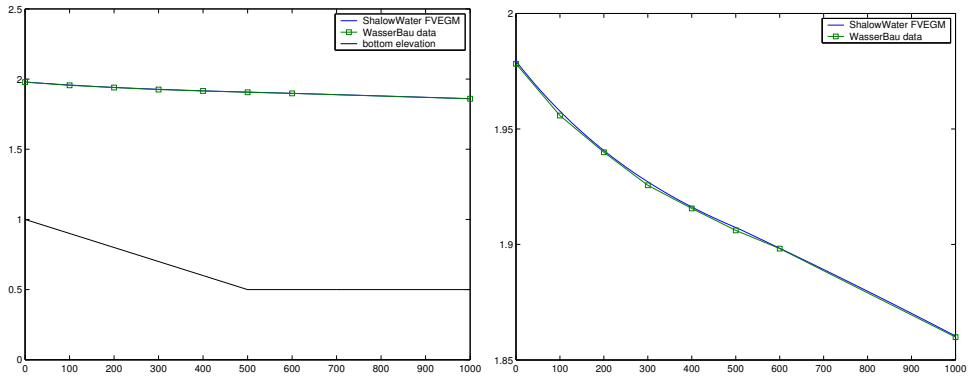

FIG. 4.2. *Comparison of the two-dimensional solution obtained by the FVEG scheme (solid line) and the one-dimensional steady solution obtained by the FEM scheme (boxes).*

Acknowledgments. The author would like to thank Ulf Teschke, Sebastian Rath and Erik Pasche, Institut for River and Coastal Engineering, TU Hamburg-Harburg, for fruitful discussions on numerous practical aspects of river flow modeling. We also thank Ulf Teschke for providing the data of his channel flow simulation.

REFERENCES

[1] N. Botta, R. Klein, S. Langenberg, S. Lützenkirchen, *Well balanced finite volume methods for nearly hydrostatic flows*, J. Comp. Phys., 196(2004), pp. 539-565.

[2] M. Fey, *Multidimensional upwinding, Part II. Decomposition of the Euler equations into advection equations*, J. Comp. Phys., 143(1998), pp. 181-199.

[3] J.M. Greenberg, A.-Y. LeRoux, *A well-balanced scheme for numerical processing of source terms in hyperbolic equations*, SIAM J. Numer. Anal., 33(1996), pp. 1-16.

[4] A. Kurganov, D. Levy, *Central-upwind schemes for the Saint-Venant system*, M^2AN, Math. Model. Numer. Anal., 36(3)(2002), pp. 397-425.

[5] R.J. LeVeque, *Wave propagation algorithms for multi-dimensional hyperbolic systems*, J. Comp. Phys., 1997(131), pp. 327-353.

[6] R.J. LeVeque, *Balancing source terms and flux gradients in high-resolution Godunov methods: The quasi-steady wave propagation algorithm*, J. Comp. Phys., 146(1998), pp. 346-365.

[7] M. Lukáčová-Medviďová, J. Saibertová, *Genuinely multidimensional evolution Galerkin schemes for the shallow water equations*, Enumath Conference, in Numerical Mathematics and Advanced Applications, F. Brezzi et al., eds., World Scientific Publishing Company, Singapore, 2002, pp. 105-114.

[8] M. Lukáčová-Medviďová, J. Saibertová, G. Warnecke, *Finite volume evolution Galerkin methods for nonlinear hyperbolic systems*, J. Comp. Phys., 183(2002), pp. 533-562.

[9] M. Lukáčová-Medviďová, K.W. Morton, G. Warnecke, *Finite volume evolution Galerkin methods for hyperbolic problems*, SIAM J. Sci. Comput. 26(1)(2004), pp. 1.-30.

[10] M. Lukáčová-Medviďová, Z. Vlk, *Well-balanced finite volume evolution Galerkin methods for the shallow water equations with source terms*, Int. J. Numer. Meth. Fluids, 2004, accepted.

[11] S. Noelle, *The MOT-ICE: a new high-resolution wave-propagation algorithm for multi-dimensional systems of conservative laws based on Fey's method of transport*, J. Comp. Phys. 164(2000), pp. 283-334.

[12] J. Shi, *A steady-state capturing method for hyperbolic systems with geometrical source terms*, M^2AN, Math. Model. Numer. Anal., 35(4)(2001), pp. 631-646.

[13] U. Teschke, *A new procedure of solving the one-dimensional Saint-Venant equations for natural rivers*, in Wasserbau fünf Jahre, E.Pasche, ed., TU Hamburg-Harburg, 2003, pp. 35-39.

[14] U. Teschke, *Zur Berechnung eindimensionaler instationärer Strömungen von natürlichen Fließgewässern mit der Methode der Finiten Elemente*, PhD Dissertation TU Hamburg-Harburg, 2003, Fortschritt-Berichte VDI, 7/ 458, 2004.